

# NO structures adsorbed on Rh(111) : theoretical approach to high-coverage STM images

**Citation for published version (APA):**

Popa, C., Flipse, C. F. J., Jansen, A. P. J., Santen, van, R. A., & Sautet, P. (2006). NO structures adsorbed on Rh(111) : theoretical approach to high-coverage STM images. *Physical Review B*, 73(24), 245408-1/10. Article 245408. <https://doi.org/10.1103/PhysRevB.73.245408>

**DOI:**

[10.1103/PhysRevB.73.245408](https://doi.org/10.1103/PhysRevB.73.245408)

**Document status and date:**

Published: 01/01/2006

**Document Version:**

Publisher's PDF, also known as Version of Record (includes final page, issue and volume numbers)

**Please check the document version of this publication:**

- A submitted manuscript is the version of the article upon submission and before peer-review. There can be important differences between the submitted version and the official published version of record. People interested in the research are advised to contact the author for the final version of the publication, or visit the DOI to the publisher's website.
- The final author version and the galley proof are versions of the publication after peer review.
- The final published version features the final layout of the paper including the volume, issue and page numbers.

[Link to publication](#)

**General rights**

Copyright and moral rights for the publications made accessible in the public portal are retained by the authors and/or other copyright owners and it is a condition of accessing publications that users recognise and abide by the legal requirements associated with these rights.

- Users may download and print one copy of any publication from the public portal for the purpose of private study or research.
- You may not further distribute the material or use it for any profit-making activity or commercial gain
- You may freely distribute the URL identifying the publication in the public portal.

If the publication is distributed under the terms of Article 25fa of the Dutch Copyright Act, indicated by the "Taverne" license above, please follow below link for the End User Agreement:

[www.tue.nl/taverne](http://www.tue.nl/taverne)

**Take down policy**

If you believe that this document breaches copyright please contact us at:

[openaccess@tue.nl](mailto:openaccess@tue.nl)

providing details and we will investigate your claim.

**NO structures adsorbed on Rh(111): Theoretical approach to high-coverage STM images**

Cristina Popa,\* C. F. J. Flipse, A. P. J. Jansen, R. A. van Santen, and P. Sautet

*Molecular Materials and Nanosystems, Schuit Institute of Catalysis, ST/SKA,**Eindhoven University of Technology, P.O. Box 513, NL-5600 MB Eindhoven, The Netherlands**and Laboratoire de Chimie, UMR CNRS 5182, École Normale Supérieure, 46 Allée D'Italie, 69364 Lyon, France*

(Received 18 January 2006; revised manuscript received 17 March 2006; published 7 June 2006)

Theoretical modeling of scanning tunneling microscopy (STM) measurements is used for the interpretation of images of nitrogen monoxide on Rh(111) surfaces in order to gain insight into the factors which control the contrast of an STM image, especially in the case of high coverage overlayers. Topographic images of NO/Rh(111) for different coverages and adsorption positions were calculated. These results were used to analyze the experimental images obtained for the  $p(2 \times 2)$ -3NO and  $p(3 \times 3)$ -7NO high coverage structures. The theoretical calculations confirm that not all NO molecules present on the surface can be observed experimentally, the image being dominated by the contribution of top NO molecules in the adlayer. In addition, the calculations reveal that destructive interference effects between molecular contributions in the tunnel current play a decisive role for the different contrast of the two high coverage structures. A general discussion of why and how the differences in the adsorbate surface configuration reflect the experimental STM images is given.

DOI: 10.1103/PhysRevB.73.245408

PACS number(s): 68.43.Bc, 68.43.Fg, 73.20.-r, 68.37.Ef

**I. INTRODUCTION**

Understanding the surface structure of a system requires investigation of its electronic, physical, and chemical properties. There are many experimental techniques used to investigate adsorbates on metal surfaces and elementary processes. Scanning tunneling microscopy (STM) is a real space experimental method, able to obtain atomic and molecular scale resolution, which has developed in recent years as a key technique in surface science. One key aspect is the ability to operate not only in vacuum but also under the presence of a gas or under a liquid. The images can provide important information about adlayer structures. However, their interpretation is often not straightforward since STM images depend both on the geometric and electronic structures of the sample. Moreover, the nature of the substrate, the geometry of the adsorbate in specific sites, and the structure of the tip apex also influence the resulting image.<sup>1</sup>

Theoretical calculations of the STM images therefore become necessary for a correct understanding of the experimental data.<sup>2-6</sup> Coupling experimental studies with theoretical approach makes it possible to obtain valuable information about the adsorption sites, bond lengths, and defects, and to determine which electronic states predominantly contribute to the observed STM pattern. Despite their strong relevance with the high pressure situation in heterogeneous catalysis, high coverage STM images have been studied less than low coverage ones. Two structural effects could indeed have importance at high coverage: the simultaneous occupation of different sites and the proximity between adsorbate molecules. The tip is probing not an individual molecule but a surface area containing several molecules.

Nitrogen monoxide adsorbed on metallic surfaces is the subject of an impressive number of publications thanks to its importance in three way catalysis, in controlling exhaust emissions, and in environmental processes.<sup>2,7-17</sup> Brown *et al.*<sup>16</sup> have extensively reviewed the results obtained for NO on metallic surfaces. Rider *et al.*<sup>17</sup> built a setup for STM

under a pressure of gas, and they observed, after dosing NO at 0.03 Torr pressure, two different areas in the STM images corresponding to two domains with very similar coverages of 0.75 and 0.78 ML NO/Rh(111) (Fig. 1). The two proposed structures— $p(2 \times 2)$ -3NO and  $p(3 \times 3)$ -7NO—are in a dynamic equilibrium. The bright spots in their STM images were tentatively assigned to NO adsorbed in the top position, in reference to the previous calculations for CO on Pd(111),<sup>5</sup> with those of the inside domain ( $3 \times 3$ ) being brighter (+0.1 Å) compared to those in the outside domain ( $2 \times 2$ ) (see Fig. 1). The proposed structure models also include NO molecules in threefold hollow positions, which are not clearly associated with a maximum in the image. These data open several questions: is the maximum in the image indeed assigned to NO molecules adsorbed on the top position? Why are the maxima in the  $p(3 \times 3)$ -7NO structure brighter? Is this from a topographic or electronic effect? How do the NO molecules in threefold hollow position contribute to the STM image?

In this paper, we present a theoretical study of the mechanism governing the contrast for STM images of NO adsorbed on a rhodium surface. We focus on the images of NO on the Rh(111) surface as a function of coverage and compare calculated with experimental results.<sup>17</sup> We first discuss the method for obtaining STM images. In the following section we show the calculated images for low coverages, isolated adsorbed NO molecules. The results of the calculations for particular adsorption sites were then used to assess the contributions to the images calculated for high coverage systems. We then analyze the results for the calculated STM images of the two structures proposed by Rider *et al.*,<sup>17</sup> and how they compare to the images with low coverage NO. Specific phenomena governing the STM contrast for high coverage adlayers are finally underlined.

**II. COMPUTATIONAL DETAILS**

Our approach combines total energy calculations for the determination of the electronic and geometric structures for

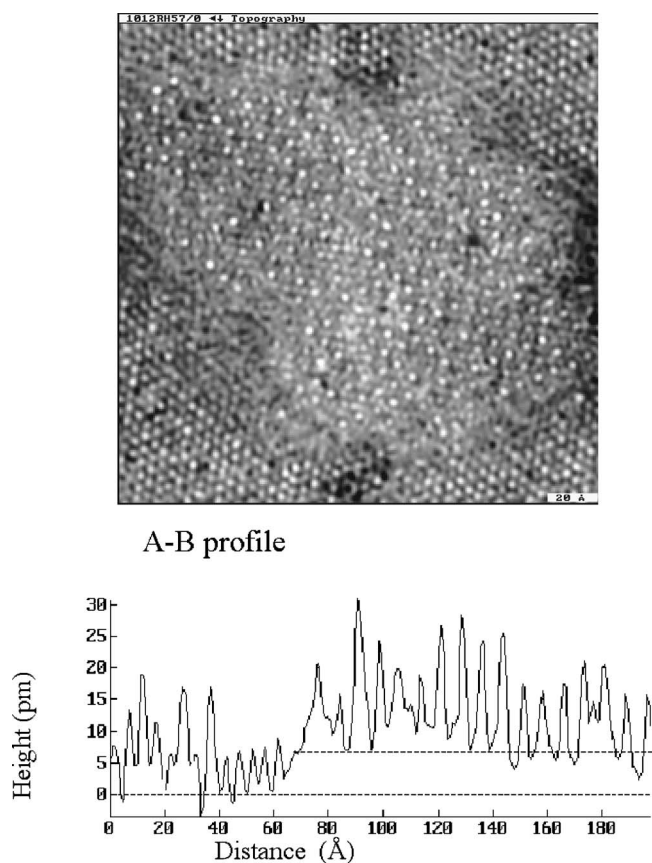


FIG. 1. Scanning tunneling microscopy images of NO/Rh(111); left:  $200 \text{ \AA} \times 200 \text{ \AA}$  STM topographic image taken in 0.03 Torr NO at  $25 \text{ }^\circ\text{C}$ ; right: profile line along A-B. Reprinted figure with permission from Ref. 17. © 2005 by the American Physical Society.

NO on Rh(111) and simulations of the STM images. The adsorption structures were optimized using density functional theory (DFT). The STM simulations were then performed from a scattering approach using a tight-binding approach, and with a complete description of the sample and tip systems. Indeed, such a tip-sample system is too large for a direct DFT calculation, and instead a Hamiltonian is used: the extended Hückel theory (EHT). In order to maintain the electronic description as close as possible to the DFT one, the EHT parameters are obtained by fitting the electronic structure with the DFT results. This requires to first recalculate the electronic structure with a localized basis set DFT code.

### A. Periodic DFT calculations

The structural optimizations were performed using the Vienna Ab Initio Simulation Package (VASP),<sup>18,19</sup> with a plane wave basis set, ultrasoft Vanderbilt pseudopotentials,<sup>20</sup> and the generalized gradient approximation (GGA)<sup>21</sup> for the exchange and the correlation energy proposed by Perdew and Wang 91.<sup>22</sup> Tests showed that the spin contribution is negligible and hence a spin-restricted approach was used.<sup>23–25</sup> With the considered pseudopotentials, a cutoff energy of 400 eV for the plane wave basis ensures a good accuracy.

For the Brillouin zone integration a MonkhorstPack  $5 \times 5 \times 1$  mesh was used.

The Rh(111) surface was modeled with the slab supercell approach. We used slabs with five metal layers, which were allowed to relax fully, and an equivalent vacuum space in the  $z$  direction between successive slabs. The optimized bulk nearest-neighbor separation of  $2.72 \text{ \AA}$  is in good agreement with the experimental value of  $2.69 \text{ \AA}$ . The NO molecules were adsorbed on both sides of the metallic slab with a  $S_2$  symmetry center to avoid long-range dipole-dipole interactions perpendicular to the surface between translational equivalent unit cells. Tests performed with different values of the cutoff energy and the number of  $k$ -points showed that the accuracy of the total energy is within  $5 \times 10^{-2} \text{ eV}$  per molecule.

### B. EHT parametrization

In the EHT approach, the one electron wave function is developed as a linear combination of atomic orbitals (AO), each of them being described by one or two Slater orbitals. Here N and O are described by their  $s$  and  $p$  AO, while Rh is represented by  $s$ ,  $p$ , and  $d$  AO. The overlap matrix elements between each AO are explicitly calculated, while the Hamiltonian matrix elements are approximated. Despite its simplicity, the EHT method is able to give an accurate description of the electronic structure after a specific parametrization procedure, where the EHT band structure and the projected density of states for each atom are fitted with the DFT band structure.<sup>26,27</sup> The parameters for bulk Rh were determined from a bulk calculation, while those for surface Rh atoms, N and O, were adjusted with the NO on Rh(111) slab calculations. Each configuration, with different NO adsorption site or coverage, was independently fitted. Two types of Rh atoms were considered in each case, bonded or nonbonded to the NO molecule.

In order to perform this fit, the atom projected density of states is needed from the DFT calculation. This is more accurately determined from a DFT calculation using a localized atomic basis set. For this purpose, the SIESTA code<sup>28–30</sup> was used, with a basis set defined by pseudo-atomic orbitals (PAOs) as generated in the code.<sup>31</sup> The geometry was kept to that determined with the plane wave approach. The Troullier-Martins scheme was used for the generation of GGA pseudo-potentials.

### C. STM calculations

To accurately describe the electron tunneling, the STM images were calculated using the GREEN 1.1 code based on scattering theory<sup>1,32,33</sup> and on Green's functions formalism.<sup>34–36</sup> The program uses a tight-binding approximation for the Hamiltonian and calculates the one-electron Green's function of the entire sample + tip system.<sup>32</sup> Both tip and sample solids are described as semi-infinite systems, and the atomic structure of the tip apex is also fully taken into account. Here a tip made of tungsten was selected, the apex being described by a ten atoms cluster oriented along the (111) direction. The optimized structure and the electronic parameters of the tip were taken from the code database.

TABLE I. NO adsorption energies, N-O and Rh-N bond lengths for different coverages and positions; positions of N and O atoms with respect to the  $z$  coordinate of the top layer of the Rh bare surface.

System	NO position	$E_{ads}$ (eV/molecule)	$d(\text{N-O})$ (Å)	$d(\text{Rh-N})$ (Å)	$z(\text{N})$ (Å)	$z(\text{O})$ (Å)
$p(2 \times 2)$ -NO $\theta = 1/4$ ML	top	-1.86	1.179	1.786	2.040	3.219
	bridge	-2.27	1.204	1.969	1.560	2.762
	fcc	-2.37	1.219	2.053	1.372	2.591
	hcp	-2.46	1.219	2.044	1.359	2.578
$p(3 \times 3)$ -NO $\theta = 1/9$ ML	top	-1.95	1.178	1.780	2.038	3.215
	bridge	-2.36	1.205	1.969	1.549	2.752
	fcc	-2.54	1.220	2.053	1.394	2.615
	hcp	-2.58	1.221	2.044	1.369	2.590
$p(4 \times 4)$ -NO $\theta = 1/16$ ML	top	-1.90	1.177	1.785	2.045	3.223
	bridge	-2.36	1.206	1.964	1.543	2.747
	fcc	-2.57	1.222	2.045	1.381	2.601
	hcp	-2.61	1.222	2.044	1.360	2.582

From the obtained Green's function, the electron transmission probability and the tunneling current can be calculated as a function of applied voltage. The tip is scanned over the surface to generate the image. Topographic images are obtained by determining for each pixel the height of the tip associated to a given current and voltage value. The convergence of the current and of the image corrugation with the number of  $k$ -points used in the calculation was tested. A cutoff radius of 40 Å was found to give a good accuracy for the  $k$ -grid.

Calculations were performed using different values for the bias voltage and current intensity. The key parameter is the tunnel resistance, defined as the ratio between voltage and current. A small gap resistance yields a small tip sample separation, and hence a large image corrugation. The conditions used in the experiments (0.5 nA and 100 mV) were here selected for all images. The trends described are similar if the gap resistance is decreased by a factor of up to 20.

### III. RESULTS AND DISCUSSIONS

#### A. NO/Rh(111) surface

Geometry optimization calculations were performed for coverages between 0.0625 and 0.78 ML (Table I). First we considered unit cells with a single NO molecule in different high symmetry adsorption sites on the surface. The  $z$  separation between NO and the Rh layer decreases from NO on top, to NO in bridge, to NO fcc, and to NO in hcp position while the N-O bond length slightly increases. This is a consequence of the larger backdonation of electrons from the Rh surface to the antibonding  $2\pi^*$  orbital of NO, when adsorbed in a higher coordination site.<sup>37,38</sup> Altogether, the  $z$  coordinate of the uppermost atom (O) decreases by 0.62–0.64 Å when moving from the top to hollow site, with a negligible difference (0.02 Å) between hcp and fcc hollow sites. The most stable adsorption sites for NO on the Rh(111) surface are the threefold hollow sites.<sup>7,39</sup> The adsorption energies increase

with decreasing coverage, especially for the threefold hollow sites, which points to repulsive lateral interactions. The hcp sites are slightly more favorable than the fcc site (0.04–0.09 eV). NO on hollow is then observed at low coverage; however, at high coverage NO occupies the top site too, and, as we will see, is associated with the main pattern in a STM image. Before considering the complex high coverage structures, we calculate the images for each site of NO for different coverages. It is very important to know the intrinsic contribution to the tunneling current of the individual molecules.

STM topographic images for NO in all high symmetry positions on the Rh(111) surface and in  $2 \times 2$ ,  $3 \times 3$ , and  $4 \times 4$  surface unit cells are shown in Fig. 2. A linear grayscale was used for each image, with black and white at positions  $z_{min}$  and  $z_{max}$ , respectively. In the same conditions of current (0.5 nA) and voltage (100 mV), and the same metallic tip, the bare Rh surface yields an image with negligible corrugation ( $3 \times 10^{-3}$  Å), the tip sample distance is 7 Å. This tip-surface separation for the bare surface is used as a reference for  $z_{min}$  and  $z_{max}$ .

The NO molecules on the top position give the largest contribution to the STM picture, i.e., the strongest corrugation (0.98 Å at low coverage). The height of the bump is strongly decreased in the case of hollow site (0.3 to 0.4 Å) at low coverage, with a similar image for fcc and hcp sites. For the NO on bridge adsorption position the images have a slightly elongated shape, in line with the pseudosymmetry of the site. If the separation between molecules is large enough ( $4 \times 4$ ) the tip height between the molecules almost coincides with that of the bare surface (zero by reference here). The slightly negative value is due to the perturbation of the metallic states from molecular adsorption.<sup>33</sup> When the separation between molecules is decreased, the molecular tails for the STM current overlap, and in between the molecules the tip picks current from them:  $z_{min}$  remains higher than the bare surface value. This effect is large when the contribution of the molecule is strong, i.e., with the top site. The value of



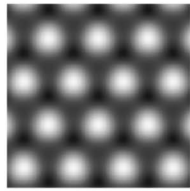
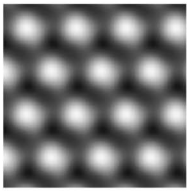
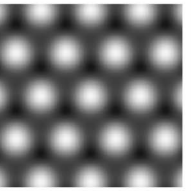
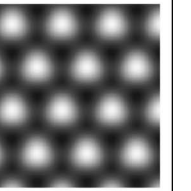
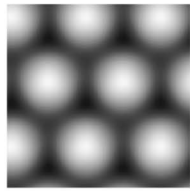
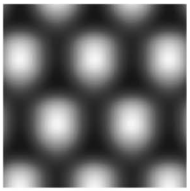
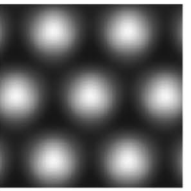
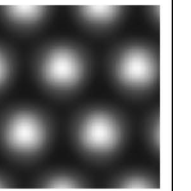
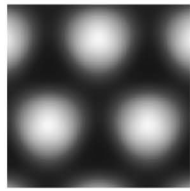
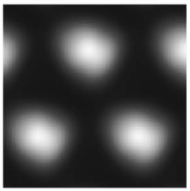
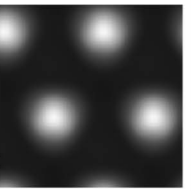
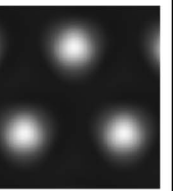
	top	bridge	fcc	hcp
Rh(2x2) 0.25 ML				
$z_{\min}(\text{\AA})$	0.65	0.25	0.20	0.11
$z_{\max}(\text{\AA})$	0.94	0.55	0.45	0.36
corrugation( $\text{\AA}$ )	0.29	0.30	0.25	0.25
Rh(3x3) 0.11 ML				
$z_{\min}(\text{\AA})$	0.16	-0.01	-0.04	-0.05
$z_{\max}(\text{\AA})$	1.00	0.57	0.38	0.31
corrugation( $\text{\AA}$ )	0.84	0.58	0.42	0.36
Rh(4x4) 0.0625 ML				
$z_{\min}(\text{\AA})$	0.03	-0.01	-0.04	-0.03
$z_{\max}(\text{\AA})$	1.01	0.57	0.36	0.29
corrugation( $\text{\AA}$ )	0.98	0.58	0.39	0.32

FIG. 2. Topographic STM calculated images  $20 \text{ \AA} \times 20 \text{ \AA}$  of NO/Rh(111) for a current of 0.5 nA and an applied voltage of 100 mV with a W(111) tip. Various adsorption sites and coverage are considered. Corrugation is defined as the total amplitude of the image,  $z_{\max} - z_{\min}$ .

$z_{\min}$  is hence strongly dependent on the molecular coverage.  $z_{\max}$  varies much less and the sign of the variation depends on the adsorption site: small decrease with coverage in the case of top site, negligible for bridge site, small increase with hollow site. This results from different (and small) interference effects between neighboring molecules for each site, as it will be detailed later.

In order to understand the influence of the adsorption site on the STM contrast, there are two effects to take into account: the geometrical (or topographic) aspect and the electronic aspect. Geometrically the NO on top has a significantly higher  $z$  coordinate than the hollow NO (by  $0.62 - 0.64 \text{ \AA}$ ). For a given tip  $z$  value, the tip-molecule overlap will hence be much larger in the case of the top site, leading to a higher tunneling probability, than for the hollow site. In the topographic image,  $z_{\max}$  is correspondingly higher when the tip is above the top site NO, with respect to the hollow site. At low coverage, the  $z_{\max}$  difference between top and hollow adsorption ranges between  $0.65 \text{ \AA}$  (fcc) and  $0.72 \text{ \AA}$  (hcp), hence remaining close to the geometric value.

The geometric aspect is not the only one, since the variation in the  $z_{\max}$  value does not completely match the vertical shift of the molecule. In addition, the molecular orbital levels are affected by adsorption, in a different way on different sites. The projected density of states on NO in the range  $[\epsilon_F, \epsilon_F + 0.1 \text{ eV}]$  is higher in the case of top NO than for the

hollow NO. Hence the tunneling probability is higher for NO top, explaining why the  $z_{\max}$  differences in the image is larger than the geometric  $\Delta z$  value. This electronic effect remains, however, small. It can be underlined that the contrast difference between fcc and hcp hollow sites is almost entirely attributed to the electronic effect, since the geometric difference is negligible. The properties of NO/Rh(111) will be used for further discussing the contribution of individual molecules to the STM images of high coverage structures.

## B. $p(2 \times 2)$ -3NO and $p(3 \times 3)$ -7NO

In this section we first describe the proposed models for the high coverage adsorption structures of NO on Rh(111). We then compare the calculated STM images with the experimental ones.<sup>17</sup>

### 1. $p(2 \times 2)$ -3NO and $p(3 \times 3)$ -7NO structures

$p(2 \times 2)$ -3NO and  $p(3 \times 3)$ -7NO can both be present on the surface in equilibrium due to the close values for the coverage (0.75 and 0.78, respectively) and adsorption energies per NO molecule. Previously the  $p(2 \times 2)$ -3NO structure was obtained from high-resolution electron-energy-loss spectroscopy and low-energy electron diffraction data.<sup>39-41</sup> It

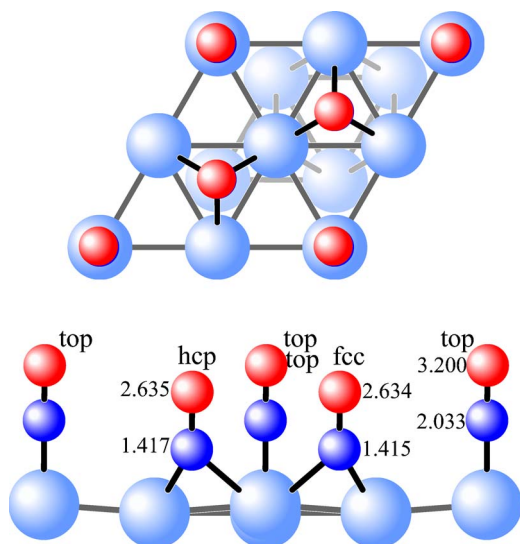


FIG. 3. (Color online) Top view and side view along the long diagonal of  $p(2 \times 2)$ -3NO. The heights of the atoms with respect to the top layer of the bare Rh surface are given in Å.

was also determined from DFT calculation by Loffreda *et al.*<sup>7</sup> and more recently by Vang *et al.*<sup>12</sup> According to the experimental data and the first calculations<sup>7</sup> the most stable configuration consists of (top+fcc+hcp) NO with all NO's in the up-right position (Fig. 3). A structure with (top+2 bridge) NO was also proposed, but the adsorption energy for this structure is 0.65 eV/molecule higher. In the second calculation<sup>12</sup> a similar (top+fcc+hcp) structure was obtained but with NO on top tilted approximately 30° from the vertical position. Our calculations agree perfectly with the first calculated structure (top+fcc+hcp), with all NO's in the up-right position. We tried to generate the structure with tilted NO on top but the optimization led us back to the up-right position.

For the  $p(3 \times 3)$ -7NO structure Rider *et al.*<sup>17</sup> proposed two possibilities, the most probable one being (top+3 fcc +3 hcp) NO molecules, and the other model (top+6 near hollow sites) NO's per unit cell. Vang *et al.*<sup>12</sup> reported for this structure a tilted (top+3 fcc+3 hcp). According to our calculations, the most stable configuration is again (top +3 fcc+3 hcp) with all NO's in the up-right position (Fig. 4).

In Table II we present the calculated values for the average adsorption energies per NO molecule and some geometrical parameters. The comparison between calculated and experimental NO adsorption energies is not straightforward. GGA DFT functionals, as PW91 used here, have been argued to overestimate the adsorption energies on transition metal surfaces.<sup>38,42,43</sup> The values for the first structure are in very good agreement with those given by Loffreda *et al.*<sup>7</sup> The experimental adsorption energy reported was  $-1.0 \pm 0.1$  eV,<sup>39</sup> but this value was obtained from temperature-programmed desorption (TPD) spectra for NO decomposition at 0.25 ML NO coverage in the presence of 0.25 ML N and 0.25 ML O atoms. There are considerable lateral interactions in this ad-layer, making it very difficult to determine experimentally the real adsorption energy of NO. Therefore the adsorption

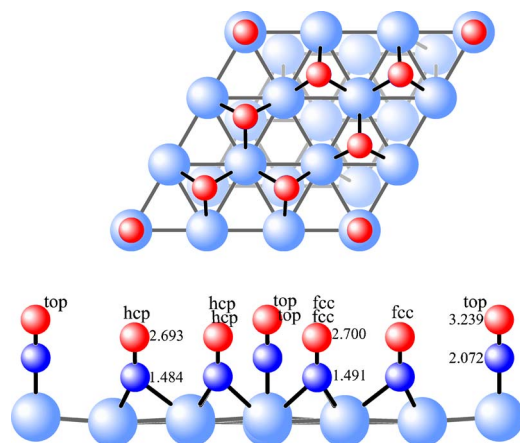


FIG. 4. (Color online) Top view and side view along the long diagonal of  $p(3 \times 3)$ -7NO. The heights of the atoms with respect to the top layer of the bare Rh surface are given in Å.

energy on a clean Rh(111) surface is much higher than the  $-1.0$  eV. In fact, our larger value of the adsorption energy reproduces the experiment if the lateral interactions are included.<sup>14</sup>

## 2. STM topographic images

The calculated STM topographic images (Fig. 5) show a strong domination of the top site NO molecule. The results can be correlated with the behavior of other systems at high coverage, where only the NO or CO molecules on top positions adsorbed on metallic surfaces were observed.<sup>1-3,5,6,12,15,44</sup> For the  $p(2 \times 2)$ -3NO structure we can observe bright regular maxima with some shadows in between. The STM image is qualitatively similar to that obtained for  $p(2 \times 2)$ -NO on top (Fig. 2, upper left image), where only top NO molecules are present. In the considered conditions (0.5 nA current and 100 mV bias voltage) the image ranges from 0.7 to 0.92 Å, hence with a corrugation of 0.22 Å. The NO's adsorbed in fcc or hcp sites are not detect-

TABLE II. Adsorption energies and geometrical parameters for  $p(2 \times 2)$ -3NO and  $p(3 \times 3)$ -7NO.  $\alpha$  is an angle,  $d$  is a bond length, and  $s$  a vertical separation.

	$p(2 \times 2)$ -3NO	$p(3 \times 3)$ -7NO
$\theta$ (ML)	0.75	0.78
$\langle E_{ads} \rangle$ (eV/molecule)	-2.09	-2.11
$\alpha(\text{Rh-N-O})$ top ( $^\circ$ )	178	180
$s(\text{Rh-N})$ top (Å)	1.791	1.785
$s(\text{Rh-N})$ fcc (Å)	1.305	1.340
$s(\text{Rh-N})$ hcp (Å)	1.307	1.330
$s(\text{N-O})$ top (Å)	1.167	1.163
$s(\text{N-O})$ fcc (Å)	1.219	1.208–1.209
$s(\text{N-O})$ hcp (Å)	1.219	1.204–1.207
$d(\text{Rh-N})$ fcc (Å)	2.069–2.077	2.043–2.118
$d(\text{Rh-N})$ hcp (Å)	2.065–2.073	2.044–2.135

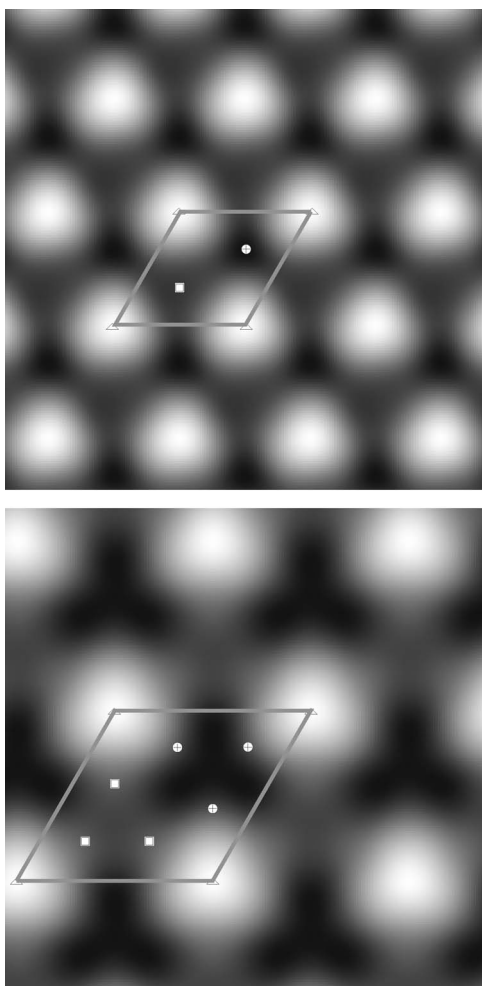


FIG. 5. Calculated STM topographic images  $20 \text{ \AA} \times 20 \text{ \AA}$  for  $p(2 \times 2)$ -3NO (top) and  $p(3 \times 3)$ -7NO (bottom) for a current of 0.5 nA, a bias voltage of 100 mV and a W(111) tip; the symbols represent the position of the NO molecules:  $\Delta$ : NO top;  $\oplus$ : NO fcc; and  $\square$ : NO hcp.

able, although the image is slightly less corrugated than for the low coverage  $p(2 \times 2)$ -NO on top.

The images for the  $p(3 \times 3)$ -7NO structure also show bright spots for NO on top and vague shadows in between. The image ranges from 0.59 to 0.98  $\text{\AA}$ , i.e., with a higher corrugation of 0.39  $\text{\AA}$ . This image should be compared with  $p(3 \times 3)$ -NO on top site in Fig. 2 (middle row, left image). Some differences appear: the bump has a smaller lateral expansion for  $p(3 \times 3)$ -7NO, and the corrugation is reduced by a factor of 2 (0.39  $\text{\AA}$  compared to 0.84  $\text{\AA}$ ) mainly from a strong increase of  $z_{\min}$  (0.59  $\text{\AA}$  compared to 0.16  $\text{\AA}$ ). Hence, although the hollow site NO molecules are not associated with a distinct bright bump in the image, they clearly affect the image from their contribution in the low (dark) part of it. The gray shadows in Fig. 5 can hence unambiguously be attributed to the contribution of hcp hollow molecules.

### 3. Decomposition of STM image in molecular contributions

In order to better understand the STM image contrast for these high coverage systems, we can decompose it into par-

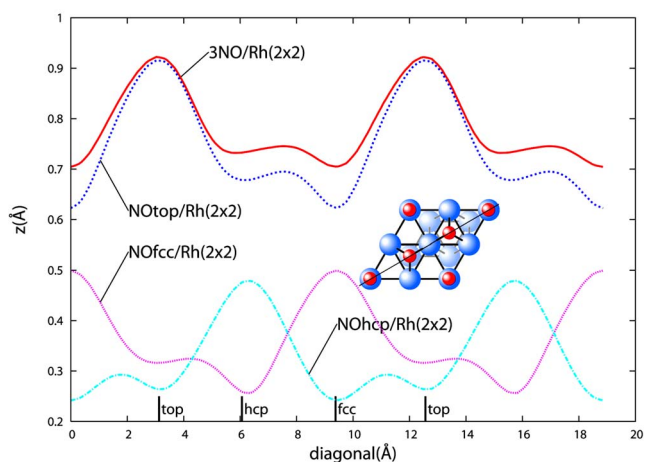


FIG. 6. (Color online) Calculated topographic diagonal scanlines for  $p(2 \times 2)$ -3NO and NO on top, fcc, and hcp at 0.5 nA current and 100 mV bias voltage. A schematic of the diagonal scan direction is given in the inset.

tial systems containing only a fraction of the adsorbed molecules. For all partial coverage structures, the molecules are kept in the geometry they occupy in the full coverage situation. This decomposition is presented with one-dimensional sections of the images, along a diagonal of the cell. Such a diagonal scan indeed crosses all high symmetry positions. The  $p(2 \times 2)$ -3NO image can be compared to the contributions of a single NO molecule in the top, fcc, or hcp hollow sites. This allows one to describe more quantitatively the trends observed earlier. Similar results were obtained for other values of the current intensity and/or bias voltage.

The decomposition for the  $p(2 \times 2)$ -3NO structure is shown in Fig. 6. The contrast for the complete system is very similar to the contribution of the NO on top molecule. As indicated above, the fcc and hcp NO molecules are invisible, their corresponding scanlines being much lower. In simple terms this means that the number of NO molecules seen in the STM image is lower than the expected value for this coverage. The maximum corrugation for the  $p(2 \times 2)$ -3NO system is somewhat smaller than for  $p(2 \times 2)$ -NO with the NO molecule only on top. In the low area of the curve ( $x = 5 - 10 \text{ \AA}$  along the diagonal), corresponding to NO fcc and hcp positions,  $p(2 \times 2)$ -3NO is slightly higher than the curve corresponding to NO on top, which is due to the contributions of the NO in fcc and hcp sites. As a consequence the curve is less corrugated than the NO on top curve. We can also underline that the secondary maximum in the complete profile, between the two bumps, is not related with the hollow molecules but with the tails of the two other top NO molecules in the other short diagonal of the rhombus unit cell.

For the case of the  $p(3 \times 3)$ -7NO structure, the seven adsorbates were separated in three subsystems: the NO on top, the 3 NO in fcc hollow sites, and the 3 NO in hcp hollow sites. The result is shown in Fig. 7. The absolute maximum again corresponds to NO on top. The other NO molecules have a lower contribution, but this time the influence of the other NO's is more important, especially in the low part of



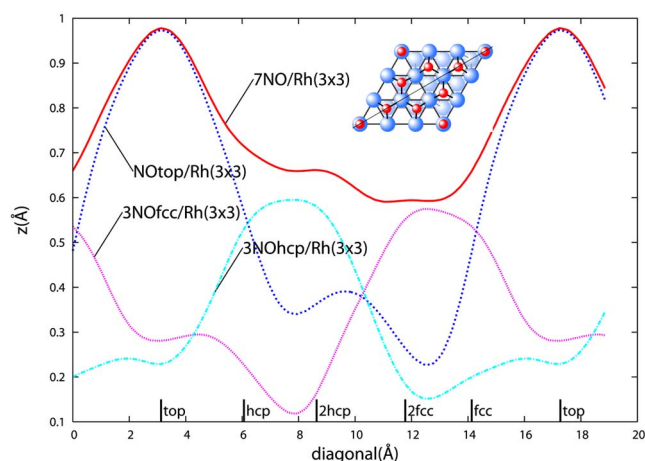


FIG. 7. (Color online) Calculated topographic diagonal scanlines for  $p(3 \times 3)$ -7NO and NO on top, 3NO fcc and 3NO hcp at 0.5 nA current and 100 mV bias voltage. A schematic of the diagonal scan direction is given in the inset.

the curve ( $x=5-15$  Å). This can be explained by two effects. First, the NO on top molecules are more separated and, second, the contribution of the 3 NO hollow molecules is slightly enhanced ( $z_{max}$  0.6 Å). As a consequence, when the tip is above the hollow molecules, their contribution is higher than that of the top NO [the lines intersect, which was not the case for  $p(2 \times 2)$ -3NO]. However, no clear secondary maximum is produced and the net result is an up-shift of the scan minimum by 0.35–0.45 Å. As in the previous case, the shallow minimum corresponds to the 3NO hcp positions and the deeper minimum corresponds to the 3NO fcc positions.

Calculated scanlines hence allow one to perform a better analysis of the STM data. The relative position of each system with respect to the individual NO's can be clearly seen from their profile. For both structures NO molecules adsorbed in hollow sites reduce the corrugation, therefore the STM images are more shallow. For the  $p(3 \times 3)$ -7NO system this effect is more consistent. The effect of NO's from hollows is more obvious in the value of the corrugation, which is almost 0.45 Å lower than for NO on top optimized in a  $p(3 \times 3)$ . However, the main feature of the images is still given by the NO on top positions.

#### 4. Analysis of interference effects

When the tip of the STM is positioned above a surface with a high coverage of molecules, the tip can simultaneously overlap with several molecules for the same  $(x, y)$  position. Hence several molecular channels are open for the electron tunneling process. Due to the wavefunction nature of the electron, these channels do not simply add but interference effects, destructive or constructive, might appear in the total current. In order to analyze this point, topographic scanlines, which represent the  $z$  coordinate of the tip, are not convenient. Hence we fixed the  $z$  of the tip and calculated the variation of the tunnel current for a bias voltage of 100 mV along the diagonal segment previously considered. The  $z$  of the tip was fixed to the value obtained on the topographic image, corresponding to the tip above the top NO mole-

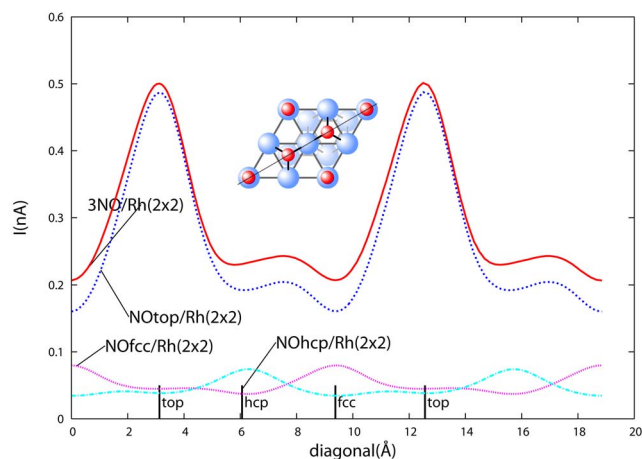


FIG. 8. (Color online) Calculated current diagonal scanlines for  $p(2 \times 2)$ -3NO and NO on top, fcc and hcp unoptimized at  $+0.922$  Å, 100 mV applied voltage.

cule for the  $p(2 \times 2)$ -3NO system. This corresponds to  $z = 0.932$  Å with the reference defined previously (7 Å), or a tip—Rh separation of 7.932 Å.

These current variations are shown in Figs. 8 for  $p(2 \times 2)$ -3NO and 9 for  $p(3 \times 3)$ -7NO, respectively. Partial currents obtained for the isolated NO on top or hollow molecules are also given. The general trend is of course similar to that observed on topographic images. NO's from the hollow sites contribute very little to the current, although their influence becomes important in the low corrugated regions. In the low region of the curve there is no maximum given by NO adsorbed in hollow sites. Furthermore, we notice an upward shift of the lines by up to 0.04 nA for  $p(2 \times 2)$ -3NO and 0.11 nA for  $p(3 \times 3)$ -7NO. When the tip is above top NO, the total current is just barely larger than that for the isolated top NO. It is, however, significantly lower than the addition of top, fcc, and hcp currents. This is also true when the tip is above the hollow NO adsorbates. Therefore the interference between molecular channels is destructive. This is associated to the out-of-phase relationship between the

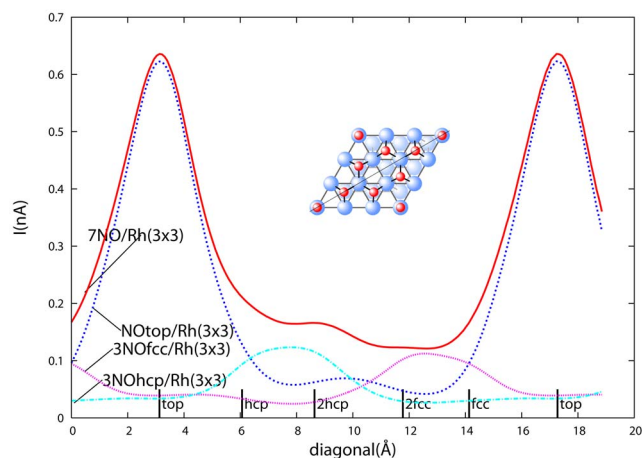


FIG. 9. (Color online) Calculated current diagonal scanlines for  $p(3 \times 3)$ -7NO and NO on top, 3NO fcc and 3NO hcp unoptimized at  $+0.922$  Å, 100 mV applied voltage.



TABLE III. Corrugations (0.5 nA applied current, 100 mV bias voltage) and currents (0.922 Å, 100 mV bias voltage) values for  $p(2 \times 2)$ -3NO and  $p(3 \times 3)$ -7NO and for the corresponding structures with only NO's on top positions.

System	3NO $p(2 \times 2)$	NO top only $p(2 \times 2)$	7NO $p(3 \times 3)$	NO top only $p(3 \times 3)$
$z_{max}$ (Å)	0.92	0.91	0.98	0.97
$z_{min}$ (Å)	0.70	0.62	0.59	0.23
corrugation (Å)	0.22	0.29	0.39	0.75
$I_{max}$ (nA)	0.50	0.49	0.64	0.62
$I_{min}$ (nA)	0.21	0.16	0.12	0.04

contributions of top and hollow NO molecules for the electronic states close to the Fermi level. A similar effect was already shown in the case of inequivalent S adsorbates on a Mo surface (Ref. 45).

### 5. Comparison between $p(2 \times 2)$ -3NO and $p(3 \times 3)$ -7NO

Table III summarizes our results for the calculated values of the corrugations and currents. Our calculations show that the STM contrast is brighter for the top NO molecule in the  $p(3 \times 3)$ -7NO, compared to the  $p(2 \times 2)$ -3NO structure. In the topographic image the maximum  $z$  value is larger by 0.06 Å, and for the current calculations the maximum current is increased by 0.14 nA. This is in very good agreement with the experimental STM images where a difference of approximately 0.1 Å is observed. This effect has the same amplitude in our calculations if only the NO on the top molecule is positioned in the  $(2 \times 2)$  or  $(3 \times 3)$  unit cell. It is therefore not related with the influence of the hollow molecules in the unit cell. It is also not related with different NO on top geometries, since, as shown in Figs. 3 and 4, the N and O  $z$  coordinates are identical in the two systems. This effect was in fact already presented in the left column of Fig. 2, where for a single NO on top molecule,  $z_{max}$  increased from 0.94 to 1.00 and to 1.01 Å when the repeat vectors are changed from  $2 \times 2$  to  $3 \times 3$  and  $4 \times 4$ , respectively. The effect is purely electronic and the key is in the different packing of the top NO molecules. The result is not completely obvious, since an increase of the NO molecule density results in a decrease of the tunnel current. We can also note that there is almost no difference between  $3 \times 3$  and  $4 \times 4$ .

In order to understand the origin of this effect, we constructed a  $4 \times 4$  unit cell with 4 NO molecules on top (see Fig. 10). This is simply a supercell representation of the  $p(2 \times 2)$ -1NO structure and gives the same result in terms of tip height or current. However, we can now understand what is the influence of top neighboring NO molecules (B) in the  $2 \times 2$  overlayer on the current of a given top NO molecule (A). The tip is positioned above the A molecule, yielding obviously a current of 0.49 nA, as indicated in Table III. Two subsystems can be constructed. The first one keeps only A and removes all B's (this is the simple  $4 \times 4$  overlayer). The current jumps to 0.57 nA. The second one removes A and keeps all B's, yielding a contribution of the neighbor molecules of 0.04 nA. Therefore the current for the (A+B) sys-

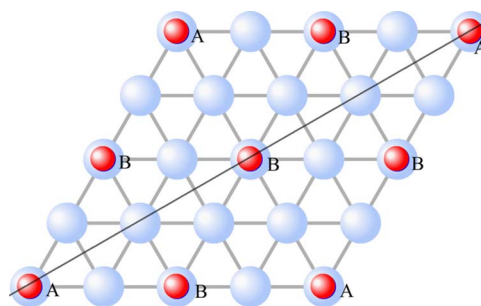


FIG. 10. (Color online) Top view of  $p(4 \times 4)$ -4NO.

tem results from a destructive interference between the contributions of the “imaged” molecule (below the tip) and that of its neighbors. An increase of the packing enhances the contribution of neighboring molecules, since they come closer to the tip. This explains the decrease of the current (and topographic height) going from  $4 \times 4$  (or  $3 \times 3$ ) to  $2 \times 2$ . In summary, the brighter contrast in the  $p(3 \times 3)$ -7NO system, compared to  $p(2 \times 2)$ -3NO is associated with a smaller destructive effect from more separated top NO molecules. The enhanced image corrugation for the  $p(3 \times 3)$ -7NO is clearly also associated with more separated NO on top molecules, the tip being able to explore more efficiently the low current region between them. It should be underlined that the nature of the interference effect between adsorbates is dependent on the type of adsorption site. From the model systems of Fig. 2, it can be seen that the interference is destructive between top site molecules, more or less neutral for bridge sites, and constructive for hollow sites. This illustrates different electronic structures at the Fermi level.

## IV. CONCLUSIONS

The theoretical simulations of STM images confirm the intuitive conclusion that for the high coverage structures of NO on Rh(111),  $p(2 \times 2)$ -3NO, and  $p(3 \times 3)$ -7NO the STM image is dominated by the contribution of the NO molecules on top adsorption sites. They also show that the  $p(3 \times 3)$ -7NO adlayer gives brighter bumps for these top NO molecules, and that the image corrugation is larger, in very good agreement with the experimental data. Simulations, moreover, give important insights for the understanding of the observed image contrast. The larger contribution for top NO has two reasons: geometric (top molecule is higher above the surface) and electronic (its electronic levels are closer to the Fermi level). As a consequence NO on top gives the highest tunneling probability. The NO molecules in the hollow sites are not associated with separated bumps in the image, but only with qualitative change of the contrast in the dark areas of the images in between the top NO bumps. For  $p(3 \times 3)$ -7NO the hollow sites play a more important role than for  $p(2 \times 2)$ -3NO in the image contrast, increasing the current in the zone in between top NO molecules, and therefore reducing the image corrugation.

A new aspect for the high (or intermediate) coverage systems is that the current is not only controlled by the molecule right below the tip, but also by the neighboring molecules

(up to distances of 6 Å), since these molecules have a non-negligible overlap with the tip electronic states. Hence several channels for tunneling are open, resulting in interference effects. This can induce specific effects in the contrast. Within the unit cell, tunneling channels are created by the top and hollow NO molecules, with a clear domination of the top NO ones. In addition, these top and hollow NO channels interfere destructively in the high coverage overlayers, decreasing even more the contribution of hollow NO molecules.

Interference effects are also active between adlayer unit cells and this explains why the  $p(3 \times 3)$ -7NO structure gives brighter features for the top NO molecules than the  $p(2 \times 2)$ -3NO one. Indeed, this is not a geometric effect, since the coordinates are almost identical in both cases. The different brightness is in fact explained by a destructive interference effect between neighboring top NO molecules. This effect is almost negligible for the  $(3 \times 3)$  separation of the top NO molecules, but becomes significant for a  $p(2 \times 2)$  packing, yielding a decreased current. Hence the  $p(2 \times 2)$ -3NO gives an attenuated brightness for the top NO

molecules. This is a purely electronic effect, specific of a nonzero coverage situation. These destructive interference effects are explained by out of phase combination between neighbor top NO molecules, from nonzero  $k$  components in the wave function at the Fermi level.

Hence simulations reveal specific effects in the STM imaging of molecules at medium or high coverage, providing an important insight for the correct interpretation of experimental images. The results have a general character and should be also important for high coverage images of other adsorbates on metallic surfaces.

## ACKNOWLEDGMENTS

This research was financially supported by the Marie Curie European Fellowship Association, the Foundation for Fundamental Research on Matter (FOM), The Netherlands, and the Netherlands National Computing Facilities Foundation, SARA. C.P. thanks Jorge Iribas Cérda, ICMM, Madrid, for his enthusiastic assistance with the software to process the STM images.

\*Electronic address: c.popa@tue.nl

- <sup>1</sup>P. Sautet, Chem. Rev. (Washington, D.C.) **97**, 1097 (1997).
- <sup>2</sup>K. H. Hansen, Ž. Šljivančanin, B. Hammer, E. Lægsgaard, F. Besenbacher, and I. Stensgaard, Surf. Sci. **496**, 1 (2002).
- <sup>3</sup>M. K. Rose, T. Mitsui, J. Dunphy, A. Borg, D. F. Ogletree, M. Salmeron, and P. Sautet, Surf. Sci. **512**, 48 (2002).
- <sup>4</sup>M.-L. Bocquet, J. Cérda, and P. Sautet, Phys. Rev. B **59**, 15437 (1999).
- <sup>5</sup>M. Ø. Pedersen, M.-L. Bocquet, P. Sautet, E. Lægsgaard, I. Stensgaard, and F. Besenbacher, Chem. Phys. Lett. **299**, 403 (1999).
- <sup>6</sup>P. Sautet, M. K. Rose, J. C. Dunphy, S. Behler, and M. Salmeron, Surf. Sci. **453**, 25 (2000).
- <sup>7</sup>D. Loffreda, D. Simon, and P. Sautet, Chem. Phys. Lett. **291**, 15 (1998).
- <sup>8</sup>D. Loffreda, D. Simon, and P. Sautet, J. Chem. Phys. **108**, 6447 (1998).
- <sup>9</sup>D. Loffreda, D. Simon, and P. Sautet, J. Catal. **213**, 211 (2003).
- <sup>10</sup>D. Loffreda, F. Delbecq, D. Simon, and P. Sautet, J. Chem. Phys. **115**, 8101 (2001).
- <sup>11</sup>E. Ozensoy, C. Hess, D. Loffreda, P. Sautet, and D. W. Goodman, J. Phys. Chem. B **109**, 5414 (2005).
- <sup>12</sup>R. T. Vang, J.-G. Wang, J. Knudsen, J. Schnadt, E. Laegsgaard, I. Stensgaard, and F. Besenbacher, J. Phys. Chem. B **109**, 14262 (2005).
- <sup>13</sup>J. H. A. Eichler, Chem. Phys. Lett. **343**, 383 (2001).
- <sup>14</sup>C. G. M. Hermse, F. Frechard, A. P. van Bavel, J. J. Lukkien, J. W. Niemansverdriet, R. A. van Santen, and A. P. J. Jansen, J. Chem. Phys. **118**, 7081 (2003).
- <sup>15</sup>K. B. Rider, K. S. Hwang, M. Salmeron, and G. A. Somorjai, J. Am. Chem. Soc. **124**, 5588 (2002).
- <sup>16</sup>W. A. Brown and D. A. King, J. Phys. Chem. B **104**, 2578 (2000).
- <sup>17</sup>K. B. Rider, K. S. Hwang, M. Salmeron, and G. A. Somorjai, Phys. Rev. Lett. **86**, 4330 (2001).
- <sup>18</sup>G. Kresse and J. Furthmüller, Comput. Mater. Sci. **6**, 15 (1996).
- <sup>19</sup>G. Kresse and J. Furthmüller, Phys. Rev. B **54**, 11169 (1996).
- <sup>20</sup>D. Vanderbilt, Phys. Rev. B **41**, 7892 (1990).
- <sup>21</sup>G. Kresse and J. Hafner, J. Phys.: Condens. Matter **6**, 8245 (1994).
- <sup>22</sup>J. P. Perdew, in *Electronic Structure of Solids'91*, edited by P. Ziesche and H. Eschrig (Akademie Verlag, Berlin, 1991), pp. 11–20.
- <sup>23</sup>A. Bogicevic and K. C. Hass, Surf. Sci. **506**, L237 (2002).
- <sup>24</sup>B. Hammer, Surf. Sci. **459**, 323 (2000).
- <sup>25</sup>B. Hammer, Faraday Discuss. **110**, 323 (1998).
- <sup>26</sup>J. Cérda and F. Soria, Phys. Rev. B **61**, 7965 (2000).
- <sup>27</sup>J. Méndez, S. H. Kim, J. Cérda, J. Wintterlin, and G. Ertl, Phys. Rev. B **71**, 085409 (2005).
- <sup>28</sup>D. Sánchez-Portal, P. Ordejón, E. Artacho, and J. M. Soler, Int. J. Quantum Chem. **65**, 453 (1997).
- <sup>29</sup>P. Ordejón, E. Artacho, and J. M. Soler, Phys. Rev. B **53**, R10441 (1996).
- <sup>30</sup>J. M. Soler, E. Artacho, J. D. Gale, A. García, J. Junquera, P. Ordejón, and D. Sánchez-Portal, J. Phys.: Condens. Matter **14**, 2745 (2002).
- <sup>31</sup>E. Artacho, D. Sánchez-Portal, P. Ordejón, and A. García, Phys. Status Solidi B **215**, 809 (1999).
- <sup>32</sup>J. C. Dunphy, P. Sautet, D. F. Ogletree, and M. Salmeron, Phys. Rev. B **52**, 11446 (1995).
- <sup>33</sup>P. Sautet, Surf. Sci. **374**, 406 (1997).
- <sup>34</sup>J. Cérda, M. A. Van Hove, P. Sautet, and M. Salmeron, Phys. Rev. B **56**, 15885 (1997).
- <sup>35</sup>J. Cérda, A. Yoon, M. A. Van Hove, P. Sautet, M. Salmeron, and G. A. Somorjai, Phys. Rev. B **56**, 15900 (1997).
- <sup>36</sup>S. Corbel, J. Cérda, and P. Sautet, Phys. Rev. B **60**, 1989 (1999).
- <sup>37</sup>H. Over, Prog. Surf. Sci. **58**, 249 (1998).
- <sup>38</sup>M. Gajdoš, J. Hafner, and A. Eichler, J. Phys.: Condens. Matter **18**, 13 (2006).

- <sup>39</sup>H. J. Borg, J. F. C.-J. M. Reijerse, R. A. van Santen, and J. W. Niemanteverdriet, *J. Chem. Phys.* **101**, 10052 (1994).
- <sup>40</sup>Y. J. Kim, S. Thevuthasan, G. S. Herman, C. H. Peden, S. A. Chambers, D. N. Belton, and H. Permana, *Surf. Sci. Lett.* **359**, 269 (1996).
- <sup>41</sup>G. A. S. I. Zasada and M. A. Van Hove, *Surf. Sci. Lett.* **418**, L89 (1998).
- <sup>42</sup>M. Mavrikakis, J. Rempel, J. Greeley, L. B. Hansen, and J. K. Nørskov, *J. Chem. Phys.* **117**, 6737 (2002).
- <sup>43</sup>B. Hammer, L. B. Hansen, and J. K. Nørskov, *Phys. Rev. B* **59**, 7413 (1999).
- <sup>44</sup>P. Cernota, K. Rider, H. A. Yoon, M. Salmeron, and G. Somorjai, *Surf. Sci. Lett.* **445**, 249 (2000).
- <sup>45</sup>A. Altibelli, C. Joachim, and P. Sautet, *Surf. Sci.* **367**, 209 (1996).